

Configurational Entropies of Lipids in Pure and Mixed Bilayers from Atomic-Level and Coarse-Grained Molecular Dynamics Simulations

Riccardo Baron,[†] Alex H. de Vries,^{†,‡} Philippe H. Hünenberger,[†] and Wilfred F. van Gunsteren^{*,†}

Laboratorium für Physikalische Chemie, Eidgenössische Technische Hochschule Zürich, CH-8093 Zürich, Switzerland, and Molecular Dynamics Group, Department of Biophysical Chemistry, University of Groningen, Nijenborgh 4, 9747 AG Groningen, The Netherlands

Received: March 15, 2006; In Final Form: May 30, 2006

Single-chain and single-fragment configurational entropies of lipid tails in hydrated lipid bilayers are evaluated from molecular dynamics simulations using the quasi-harmonic approximation. The entropy distribution along individual acyl tails is obtained and compared to that of corresponding hydrocarbon chains in the liquid phase. We consider pure dipalmitoylphosphatidylcholine and mixed dioleoylphosphatidylcholine/dioleoylphosphatidylethanolamine bilayers. The systems are modeled at different levels of spatial resolution: In an atomic-level (AL) model all (heavy) atoms are explicitly simulated; in a coarse-grained (CG) model particles (beads) representing groups of covalently bound atoms are used, which map approximately four non-hydrogen atoms to one interaction site. Single-chain and single-fragment entropies and correlations between the motions of (single) acyl chains are compared. A good correspondence is found between the flexibility of the AL and CG models. The loss in configurational entropy due to the reduction in the number of degrees of freedom upon coarse-graining of the model is estimated. The CG model shows about 4 times faster convergence of the chain entropies than the more detailed AL model. Corrections to the quasi-harmonic entropy estimates were found to be small for the CG model. For the AL model, the correction due to mode anharmonicities is small, but the correction due to pairwise (supralinear) mode correlations is sizable.

Introduction

Dynamics and flexibility play a key role in the function of many biological systems. For example, proteins that are functional, yet unstructured under physiological conditions, are surprisingly abundant in eukaryotes.^{1–4} Similarly, cell membranes are remarkably flexible architectures^{5–8} capable of enclosing and protecting the cell constituents, while adapting to allow for processes such as signaling,⁹ recognition,¹⁰ and transport.^{11,12} Typical bacterial cells are very complicated molecular systems, reaching sizes of 10^4 – 10^5 nm in diameter and containing several thousand different sorts of molecules. At least a thousand of these components are molecules of “small” size (nanometer scale). The remaining ones are macromolecules, in large majority lipids, nucleic acids, and proteins. The impact of relatively small molecules on the mechanical and dynamical characteristics of cell membranes can be successfully studied by combining knowledge from experiments^{13,14} with computer simulations of model systems in atomic-level (AL) detail.^{15–19} However, the investigation of large-scale phenomena (e.g., membrane fusion and phase separation) currently requires a more coarse-grained (CG), mesoscopic level of detail.^{20–29}

The flexibility and fluidity of biological membranes is reflected in the hydrocarbon chain order parameters, which can be measured by nuclear magnetic resonance (NMR; see refs 13 and 30–35) and electron spin resonance (ESR; see refs 36 and 37) experiments using spin-labeled lipids as spectroscopic

probes. Both methods estimate the average orientation of the CH_2 segments along the chain relative to the bilayer normal, which can be related to the extent of (local) ordering of the lipid tails. Yet, the exact meaning of these measurements is still a subject of debate,^{38,39} and the interpretation of order parameters in terms of membrane thermodynamics and microstructure is a long-standing problem.⁴⁰ From a theoretical point of view, order parameters can be calculated from molecular dynamics (MD) simulation trajectories,⁴¹ and agreement with experimental data has been observed in many cases.^{42–44}

The dynamical characteristics of lipid motions within a bilayer are expected to vary with the depth along the bilayer normal, depending on the local extent of ordering of the lipid segments at a given depth and on their specific relative motions.^{8,45,46} The charged phosphate headgroups interact with the (intracellular or extracellular) polar aqueous environment. The restricted motions of the headgroups take place in an ordered environment, where lateral diffusion occurs on a long time scale.⁴⁷ The motions of the lipid tails occur in a highly fluid environment^{7,48–51} that enables thermally enhanced undulatory and peristaltic motions.^{52–54} The order parameters associated with different segments of the lipid tails provide information about the anisotropy in the interior of the bilayer. Due to the complexity (i.e., high number of degrees of freedom) of the disordered fluid states of lipid systems, only highly simplified models have been considered to correlate experimental quantities to structural and dynamical parameters (e.g., the diamond lattice model; see refs 30 and 55). Insight into the underlying microscopic behavior of the lipid tails in a bilayer might be obtained from the knowledge of the configurational space accessible to segments of the lipids at given physico-chemical conditions. The configu-

* Author to whom correspondence should be addressed. Phone: +41-1-6325501. Fax: +41-1-6321039. E-mail: wfvgn@igc.phys.chem.ethz.ch.

[†] Eidgenössische Technische Hochschule Zürich.

[‡] University of Groningen.

rational entropy is the physical quantity measuring the configurational space available to a molecular system or to a subset of its atoms. A number of relevant structural parameters are known from experiment for different lipids,⁵¹ but unfortunately no direct estimate of the configurational entropy is accessible, because calorimetric studies only measure the total change in entropy associated with a given process.⁵⁶ Although changes in NMR-derived order parameters can be related to changes of configurational entropy for proteins,^{57–60} corresponding studies have not been reported to date for lipid systems. A notable exception is an electron paramagnetic resonance (EPR) study of a dipalmitoyl-lecithin model membrane that relates ethanol-induced perturbations of the signal to changes in configurational entropy of the system,⁶¹ suggesting that the configurational entropy is the driving force for the influence of ethanol on the gel/ripple and ripple/fluid structural equilibria in the bilayer.

Computer simulations based on AL models provide a detailed microscopic picture of the properties of pure lipid bilayers^{15,42,54,62–69} and of mixed (binary) bilayers^{44,70,71} and valuable structural and dynamical insight not accessible through experimental techniques. The high computational cost of such simulations can be a drawback, because most biologically relevant events occur on (nowadays) prohibitive system size or/and simulation time scales. In the case of membrane AL simulations, typical system sizes are on the order of 10^2 lipid molecules, corresponding to a bilayer surface on the order of tens of square nanometers. For such systems, simulations are commonly carried out for tens of nanoseconds.^{54,66,72} Although few simulations of larger bilayer systems have been reported to date,^{15,65,67} computational studies of biological membranes should cover size scales of 10^3 or more lipids in the coming years. However, many interesting features of biological membranes (e.g., domain formation, bilayer fusion, cooperative motions associated with phase changes) are still largely unexplored through AL models due to limitations in either size or time scales.

For this reason, in recent years, there has been a steadily growing effort in the development of CG models for surfactants,^{73,74} polymers,^{75–77} and biomolecular aggregates.⁷⁸ Several approaches have been followed to provide a semiquantitative description of the properties of lipids^{20,23–29,79–82} and multi-component systems (e.g., mixed phospholipid/cholesterol bilayers by Izvekov and Voth²⁹). These models consist of beads (also called superatoms or interaction sites with mass) representing groups of atoms, monomers, or even several monomeric units. These beads interact through an effective potential energy function (force field) that takes into account the effects of the omitted degrees of freedom in a mean-field manner. With CG models the size-scale and time-scale dependence of the system properties can be explored.^{20–29,80–82} Subsequently, a focused AL study permits investigation of the corresponding molecular details. This is an appealing procedure, for instance, (i) in cases where an AL simulation would be excessively expensive or/and (ii) to obtain equilibrated atomistic structures of slowly relaxing systems. In the latter case, the system is constructed and equilibrated using the CG model, and the final CG coordinates are subsequently mapped to the AL model. The latter model can then be simulated for a comparatively short simulation time so as to compute structural, thermodynamic, and dynamical properties that require atomistic detail. The performance of a CG model in practical applications depends mainly on the chosen coarse-graining procedure, including (i) the model resolution (how many AL particles are mapped to one CG bead), (ii) the mapping procedure (how the bead

positions are defined as a function of the coordinates of the constituting AL particles), (iii) the potential energy function entering into the CG Hamiltonian, and (iv) the experimental and/or AL simulation properties against which the CG model was optimized. For any possible coarse-graining procedure, the average molecular structure and the corresponding structural fluctuations (flexibility) should be considered when validating a CG model.

The configurational spaces sampled by two molecular models based on different resolution scales can also be compared by calculating the associated configurational entropies. A method to estimate configurational entropies from MD simulations under a quasi-harmonic approximation (using internal coordinates) was first introduced by Karplus and Kushick⁸³ and further extended by others.^{84–86} As suggested by Schlitter,⁸⁷ the method can be applied on the basis of Cartesian coordinates. Two variants of the quasi-harmonic analysis in Cartesian coordinates have been suggested. In the most recent version of Andricioaei and Karplus,⁸⁸ the quasi-harmonic entropy is estimated by diagonalizing the covariance matrix and applying the exact quantum-mechanical equation for the entropy of a one-dimensional harmonic oscillator to the corresponding eigenvalues. In the original approach of Schlitter,⁸⁷ the diagonalization process is substituted with a determinant calculation, and the correct quantum-mechanical formula for the entropy is replaced by an approximate heuristic expression (which slightly overestimates the exact result). In practice, the two alternative formulations result in very similar entropy estimates.⁸⁶ Although the Schlitter formula is slightly less accurate and does not provide the quasi-harmonic modes of the system, it is computationally less expensive, for which reason it is used in the present work. An exception is made for dipalmitoylphosphatidylcholine (DPPC) lipids for which a quasi-harmonic analysis is also reported, and anharmonicity and correlation corrections are additionally estimated, from simulations at both the AL and the CG levels of resolution. A detailed description of the quasi-harmonic assumption and of the corresponding corrections for anharmonicity and correlation effects has been recently reported.⁸⁶ A summary about previous applications of the Schlitter and quasi-harmonic approaches to estimate configurational entropies from (bio)molecular simulations can also be found therein.

In the present study, the configurational entropy is calculated for acyl chains in lipid bilayers of different compositions. A dipalmitoylphosphatidylcholine (DPPC) bilayer is investigated as a reference case, because bilayers of this lipid have been most widely studied both experimentally and theoretically. Additionally, prompted by a recent study of the properties of dioleoylphosphatidylcholine/dioleoylphosphatidylethanolamine (DOPC/DOPE) bilayers as a function of phosphatidylcholine/phosphatidylethanolamine (PC/PE) headgroup composition,⁴⁴ the configurational entropies of acyl chains in these mixed bilayers are also estimated. Two types of models are used for these investigations. The first model is the classical GROMOS AL model,⁸⁹ where each atom in a molecule is represented by one interaction site except aliphatic groups, for which aliphatic CH_n groups are treated as one single interaction site (i.e., united atom approach). The second model is the CG model proposed by Marrink et al.,²⁷ which maps approximately four non-hydrogen atoms to one interaction site and has been optimized to model lipid aggregates in water. To keep this model as simple as possible, the CG force field was based on only five types of pair-interaction parameters and equal bead masses (72 u).²⁷ The same two models have been the subject of a recent comparative study of hydrocarbon liquids, which showed that the CG model

consistently maps to the corresponding AL model, and provided an estimate of the configurational entropy loss associated with the coarse-graining procedure.⁹⁰ The same study also pointed out possible deviations between the AL and the CG representations of the local structure of hydrocarbons in the liquid phase.

The present article addresses several aspects concerning simulations of lipid bilayers at different levels of resolution and the corresponding calculations of configurational entropies. (1) Methodological: what is the minimal simulation time required for the acyl chains of a single lipid to sample their accessible configurational space? (2) Biophysical: what is the nature of the lamellar state of lipid bilayers? How homogeneous is the distribution of the configurational entropy among the lipid chains in mixtures of different compositions? (3) Simplification of the model: to what extent does the CG model represent the AL model?

The entropy estimates are based on the (mass-weighted) covariance matrix of atomic Cartesian coordinates, because this allows not only for the calculation of the (approximate) single-chain configurational entropy of an entire acyl chain but also for the evaluation of the (approximate) single-fragment configurational entropy for different subsets of atoms (fragments). Thus, the distribution of configurational entropy along the chains and the correlation of the motions among subsets of solute atoms may be estimated. It should be kept in mind, however, that these contributions are not additive; i.e. the overall entropy of a lipid tail is not the sum of the single-fragment entropies calculated for all constituting fragments, due to the presence of interfragment correlations. Similarly, the entropy of a bilayer is not the sum of the single-chain entropies of the constituting lipids, due to the presence of intermolecular correlations. These restrictions will be implicitly underlined by the use of the terms “single-chain” and “single-fragment” entropies (see Methods section). To evaluate the rotational contribution to the configurational entropies, we make use of different procedures to superimpose successive molecular configurations along the simulated trajectories, as described previously.^{86,90} Finally, on the basis of a method recently proposed,⁸⁶ we quantify mode anharmonicity and pairwise (supralinear) mode correlation corrections to the quasi-harmonic entropy estimate in the specific case of DPPC lipid tails, to (i) investigate the validity of the assumptions underlying both the Schlitter⁸⁷ and quasi-harmonic^{83,86} approaches and (ii) compare the magnitudes of these effects between the AL and the CG models.

Methods

Molecular Dynamics Simulations. Trajectories for the lipid bilayer systems were generated using the MD package GROMACS (version 3.0.; ref 91), the AL force field by Berger et al.,⁶² and the compatible SPC water model⁹² and have been described in detail in ref 66 for pure DPPC (system F) and in ref 44 for DOPC/DOPE mixtures. The corresponding trajectories for the CG model were generated based on the CG force field by Marrink et al.²⁷ All (AL and CG) systems were simulated in a rectangular periodic box under isothermal–isobaric conditions, by separately coupling the temperature of solute and solvent degrees of freedom to a heat bath (coupling time 0.1 ps) and by coupling the pressure to a bath at 1 atm via isotropic coordinate scaling⁹³ (coupling time 0.5 ps, isothermal compressibility 0.46×10^{-3} (kJ mol⁻¹ nm⁻³)⁻¹). All MD simulations were initialized with atomic (AL) or bead (CG) velocities taken from a Maxwell–Boltzmann distribution at the desired temperature. Newton’s equations of motion were integrated using the leapfrog algorithm⁹⁴ with a time step of 5 (AL) or 40 (CG)

fs, respectively. Overall system translation and rotation were removed at every step. In the AL model, bond lengths were constrained using the LINCS algorithm,⁹⁵ and the nonbonded interactions were truncated at a distance of 1.4 nm, updated every time step in the range of 0.0–0.9 nm and every five steps in the range of 0.9–1.4 nm, using a twin-range cutoff scheme.⁹⁶ A reaction-field correction⁹⁷ was applied to account for the neglected electrostatic interactions beyond 1.4 nm, using a dielectric permittivity of 66 for the SPC water model. The CG model differs from the AL one in that (i) no constraining procedure is applied to pseudo-bond-lengths (which are described by harmonic springs), (ii) Lennard-Jones interactions between second nearest neighbors are not excluded, (iii) no dihedral-angle potential energy term is applied for 1–4 interactions, (iv) the standard GROMACS shift function⁹¹ is applied to the Lennard-Jones potential energy term, and (v) a nonbonded interaction cutoff radius of 1.2 nm was used (AL, 1.4 nm). Simulation trajectories analyzed in this study come from different sources, as summarized in Table S1 of the Supporting Information. For AL DPPC, a 25 ns trajectory initiated from an equilibrated system (1 ns) was analyzed (system F in ref 66, consisting of a total of 2×64 lipids). For AL DOPC and DOPC/DOPE mixtures, 40 ns trajectories initiated from equilibrated systems (1 ns) were analyzed (ref 44, consisting of a total of 2×64 lipids). For both types of bilayers, the systems contained approximately 30 water molecules per lipid, corresponding to the full hydration limit.⁴⁴ Analogously, a 30 ns trajectory for AL DOPE was analyzed. The corresponding CG systems for pure DPPC and DOPC have compositions and sizes (up to 2×256 lipids) specified in the Results and Discussion section. Simulations of *n*-hexadecane (C16) and *cis*-9-octadecene (C18:c9) in the isotropic liquid state with AL as well as CG models served as a reference to assess the changes in the configurational space available to lipid tails in bilayers. For these simulations an initial equilibration phase of 10 ns was followed by sampling periods of lengths (specified in the Results and Discussion section) up to 200 ns (AL simulations) or 1 μ s (CG simulations). The entire sampling periods were used for analysis.

Entropy Calculations. Configurational entropy calculations were performed following the formulation of Schlitter,⁸⁷ unless otherwise specified. As discussed elsewhere⁸⁶ this analysis provides an approximate value (upper bound) S to the true configurational entropy S_{true} of the simulated system

$$S_{\text{true}} < S = \frac{k_B}{2} \ln \det \left[\mathbf{1} + \frac{k_B T e^2}{\hbar^2} \mathbf{D} \right] \quad (1)$$

where k_B is Boltzmann’s constant, T the absolute temperature, e Euler’s number, and \hbar is Planck’s constant divided by 2π . Here, \mathbf{D} is the covariance matrix of mass-weighted atomic Cartesian coordinates, defined as

$$\mathbf{D} = \langle [\mathbf{M}^{1/2}(\mathbf{r} - \langle \mathbf{r} \rangle)] \otimes [\mathbf{M}^{1/2}(\mathbf{r} - \langle \mathbf{r} \rangle)] \rangle \quad (2)$$

where \mathbf{r} is the $3N$ -dimensional Cartesian coordinate vector of the N particles (atoms or beads) considered for the entropy calculation after least-squares fitting onto a reference structure, \mathbf{M} is the $3N$ -dimensional diagonal matrix containing the masses of these particles, broken brackets denote ensemble averaging, and the notation $\mathbf{a} \otimes \mathbf{b}$ stands for the matrix with elements μ, ν equal to $a_\mu \cdot b_\nu$. For all systems considered, the initial system configuration (after equilibration) was used as a reference structure to perform the least-squares fitting of trajectory configurations.

TABLE 1: Reference Code Definitions for the Atom Sets Used in Estimating the (Single-Chain or Single-Fragment; Internal or Internal Plus Rotational) Configurational Entropy $S_{\text{fit}}^{\text{type}}(\text{cov})$ and Nomenclature Used for the Quasi-Harmonic Entropy S_{qm}^{h} and its Corrections^a

type	description
i	internal configurational entropy (overall translation and rotation removed; eq 1)
ir	internal plus rotational configurational entropy (overall translation removed)
r	rotational entropy (eq 3)
ip	internal configurational entropy per particle
irp	internal plus rotational configurational entropy per particle
fit and cov	description
sn1	sn1 lipid tail
sn2	sn2 lipid tail
sn1 + 2	sn1 lipid tail + sn2 lipid tail
ch	alkane or alkene or acyl chain
fc	fragment of the chain/tail (subsets of the previous fit and cov sets)
definition	quasi-harmonic entropy and its corrections ^b
S_{qm}^{h}	quasi-harmonic entropy based on the formula for a quantum-mechanical harmonic oscillator
$\Delta S_{\text{cl}}^{\text{ah}}$	corresponding (additive) correction for anharmonicity in the quasi-harmonic modes, evaluated at the classical level
$\Delta S_{\text{cl}}^{\text{pc}}$	corresponding (additive) correction for pairwise (supralinear) correlation among the quasi-harmonic modes, evaluated at the classical level
S^{ctd}	corrected value ($S^{\text{ctd}} = S_{\text{qm},\text{o}}^{\text{h}} + \Delta S_{\text{cl}}^{\text{ah}} + \Delta S_{\text{cl}}^{\text{pc}}$)

^a A reference code is given for the type of estimate (type) and for the sets of atoms used for the configurational fitting (fit) and the mass-weighted covariance matrix calculation (cov). See the Methods section for definitions. ^b As defined in ref 86.

To define the notation unambiguously, the symbol $S_{\text{fit}}^{\text{type}}(\text{cov})$ will be used to denote an entropy estimated from the covariance matrix for the atoms defined by the cov reference code, using a least-squares fit of trajectory configurations onto the reference structure based on the atoms defined by the fit reference code, while the type reference code indicates how the fitting procedure is performed. Atoms in the fit set may be the same as those in the cov set but may also differ. In the present work, the cov set is always identical to or a subset of the fit set. In practice, five alternative sets of particles were used for cov and fit, as summarized in Table 1, namely, (i) the sn1 tail of a lipid molecule, including all the simulation particles from the carbonyl carbon to the last atom in the tail (reference code sn1), (ii) the corresponding sn2 tail of a lipid molecule (reference code sn2), (iii) the particles of both sn1 and sn2 tails of a lipid molecule (reference code sn1 + 2), (iv) the alkane or alkene chain of a particular hydrocarbon molecule (based on results from a previous study of liquid hydrocarbons)⁹⁰ or a given acyl chain of a lipid molecule (reference code ch), and (v) a fragment of the chain for any of the sets described above (reference code fc; for example, see Figure 1).

To investigate the separate contributions of internal and rotational degrees of freedom to the entropy, two alternative fitting procedures were used in the superposition of successive trajectory structures onto the reference one, as summarized in Table 1 (type reference code). In the first one, the molecular configurations were superimposed via a translational and rotational least-squares fit,⁹⁸ thus excluding the rotational motion from the calculated (single-chain or single-fragment) configurational entropies.⁹⁹ This yields an internal (type i) or internal-per-particle (type ip) entropy (the entropy divided by the number of particles in the cov set). In the second one, a translational superposition of fragments or chains was performed without applying any rotational transformation, thus including the rotational motion in the calculated (single-chain or single-fragment) configurational entropies. This yields an internal plus rotational (type ir) or internal plus rotational per particle (type irp) entropy. The relative contribution of overall rotation $s_{\text{fit}}^{\text{r}}(\text{cov})$ to the total entropy (expressed in percent) may be estimated from the difference between the entropies calculated

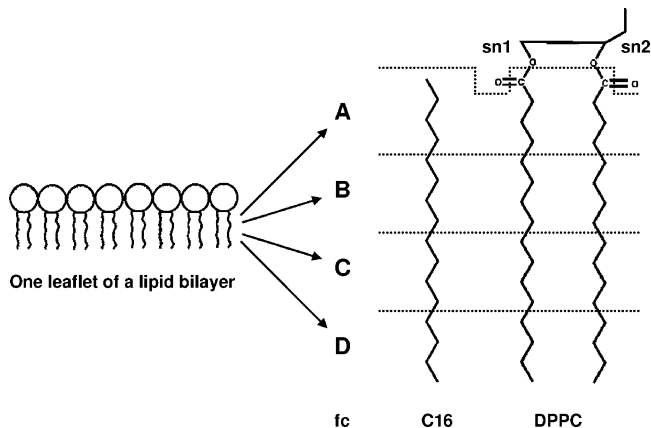


Figure 1. Definition of the fragments (fc = A, B, C, D) of acyl and hydrocarbon chains for hexadecane (C16) chains and dipalmitoylphosphatidylcholine (DPPC) tails. Dotted lines indicate fragment boundaries. Mapping of the AL model for comparison with the CG equivalent is done by calculating the centers of mass of the fragments indicated.

using the two fitting procedures, i.e., as⁹⁰

$$s_{\text{fit}}^{\text{r}}(\text{cov}) = \frac{S_{\text{fit}}^{\text{ir}}(\text{cov}) - S_{\text{fit}}^{\text{i}}(\text{cov})}{S_{\text{fit}}^{\text{ir}}(\text{cov})} \times 100 \quad (3)$$

As pointed out earlier, the latter estimates are approximate (probably representing upper bounds), due to intrinsic limitations of the quasi-harmonic approach to capture rotational contributions to the absolute entropy (interpreted as superposition of uncorrelated harmonic motions along the individual Cartesian coordinates; see refs 86 and 90).

The decrease in entropy due to correlation in the motions of two subsets i and j of atoms can be calculated as¹⁰⁰

$$S_{\text{fit}}^{\text{type}}(i,j) = S_{\text{fit}}^{\text{type}}(i+j) - S_{\text{fit}}^{\text{type}}(i) - S_{\text{fit}}^{\text{type}}(j) \quad (4)$$

where the entropy $S_{\text{fit}}^{\text{type}}(i+j)$ includes all the correlations between the atoms in the subset $(i+j)$, the type and fit sets are the same for the calculation of the three terms, and the subsets i and j are not diffusing relative to each other. The correlation

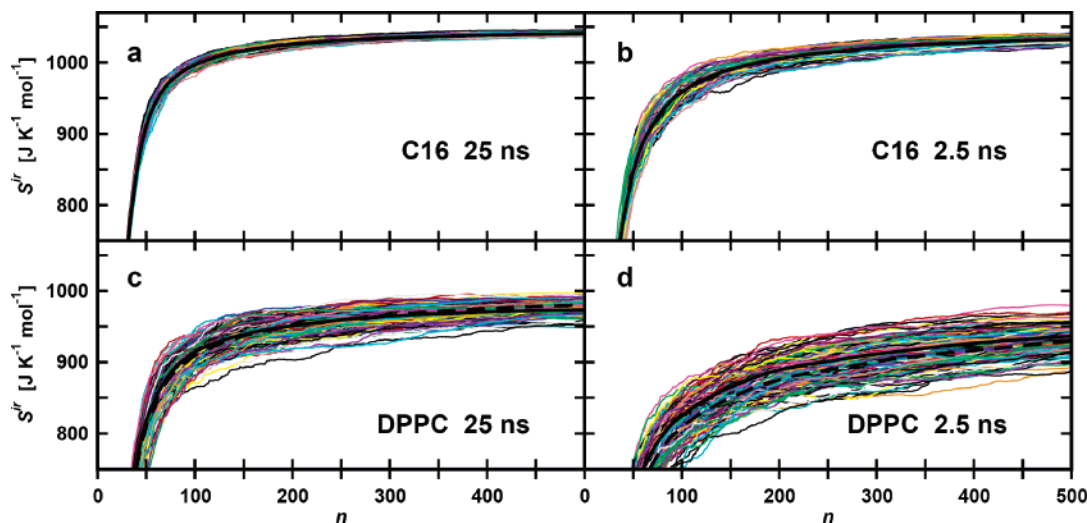


Figure 2. Single-chain configurational entropies as a function of the number n of configurations included in the calculation (AL model). For each of the 128 C16 molecules, the internal plus rotational entropies $S_{\text{ch}}^{\text{ir}}(\text{ch})$ (colored lines) and their mean value (thick black line) are shown as calculated from $n = 0 \dots 500$ trajectory configurations collected over (a) 25 and (b) 2.5 ns of a simulation of liquid C16 at 323 K (ref 90). The corresponding $S_{\text{sn1}}^{\text{ir}}(\text{sn1})$ and $S_{\text{sn2}}^{\text{ir}}(\text{sn2})$ entropies for each of the 128 lipid tails of DPPC are reported for 64 DPPC molecules (colored lines), collected over (c) 25 and (d) 2.5 ns of simulation of a hydrated DPPC bilayer at 323 K. The average values (over all lipid molecules) for the sn1 (thick black line) and sn2 (thick dashed black line) tails are also shown. See Table 1 for definition of entropy codes and Methods section for configurational entropy nomenclature.

entropies reported in this study were calculated for individual pairs of acyl chains and then averaged over the entire ensemble of lipids considered. The reported configurational entropy estimates are the average values of the (single-chain or single-fragment) entropies for the set of molecules simulated, unless otherwise specified. Corresponding error bars are evaluated as twice the standard deviation from the mean.

Anharmonicity and Pairwise (Supralinear) Correlation Corrections to the Quasi-Harmonic Entropy. To quantify anharmonicity and pairwise (supralinear) correlation corrections to the estimated entropies in the case of AL and CG DPPC systems, configurational entropies were also estimated based on a quasi-harmonic analysis.⁸⁶ This analysis was performed by calculating the solute mass-weighted covariance matrix (based on all particles in the single molecule considered) in Cartesian coordinates after least-squares fit superposition⁹⁸ of all single-molecule configurations of a (AL or CG) trajectory onto the reference structure (the initial configuration of the sampling trajectory) to eliminate overall translation and rotation.⁹⁹ The quasi-harmonic entropy estimate (S_{qm}^{h} ; see Table 1) was obtained from the entropy of a multidimensional harmonic oscillator with the same mass-weighted covariance matrix (using the appropriate quantum-mechanical formula instead of the heuristic expression of eq 1). The six (nearly zero) eigenvalues corresponding to the suppressed rigid-body motion were omitted from the analysis. Entropy corrections for anharmonicities in the quasi-harmonic modes ($\Delta S_{\text{cl}}^{\text{ah}}$; see Table 1) and for pairwise (supralinear) correlation among the modes ($\Delta S_{\text{cl}}^{\text{pc}}$; see Table 1) were evaluated at the classical level as in section 2.4 of ref 86. The anharmonicity corrections were calculated by summing the corresponding per-mode values up to eigenvector 50 ($\Delta S_{\text{cl,AL}}^{\text{ah}}$; out of 144 or 90 non-vanishing eigenmodes, for all DPPC lipid atoms or DPPC sn1 + sn2 tails, respectively) or 24 ($\Delta S_{\text{cl,CG}}^{\text{ah}}$; out of 30 non-vanishing eigenmodes, for all DPPC lipid beads), i.e., in the domain where the classical approximation is valid and where the anharmonicity effects are significant (see eq 47 and Figure 10 in ref 86). The pairwise (supralinear) correlation corrections were calculated using all pairs of non-vanishing eigenmodes (see eq 49 in ref 86). Additional information on

the underlying theory, nomenclature, assumptions, approximations, and practical implementation can be found elsewhere.⁸⁶

Results and Discussion

Convergence of Single-Chain Configurational Entropies in the AL Model. The single-chain internal plus rotational entropies S^{ir} as a function of the number of configurations included in the calculation are displayed in Figure 2 for a selection of the systems considered (AL model). In Figure 2a, the build-up curves of the internal plus rotational configurational entropies $S_{\text{ch}}^{\text{ir}}(\text{ch})$ of each chain in a system consisting of 128 hexadecane (C16) molecules in the liquid phase at 323 K are shown.⁹⁰ The results are obtained from 500 configurations collected over 25 ns. The single-chain entropies are seen to build up similarly for all chains; i.e., the spread between the curves for the different molecules is small and decreases upon increasing the number of configurations included in the calculation. On the basis of the average build-up curve for all molecules, the estimated entropy is found to be well converged within a simulation time of 25 ns (243 configurations are sufficient to account for 99% of the final entropy value). The curves for the same system calculated from 500 configurations collected over a shorter time interval of 2.5 ns are displayed in Figure 2b. Here also, adequate convergence is reached within the simulation period (310 configurations are sufficient to account for 99% of the final entropy estimate). The corresponding curves for $S_{\text{sn1}}^{\text{ir}}(\text{sn1})$ and $S_{\text{sn2}}^{\text{ir}}(\text{sn2})$ for the sn1 and sn2 tails of lipid molecules in a DPPC bilayer are shown in Figures 2c and 2d. They level off more slowly compared to liquid C16. For an interval of 25 ns, they are moderately converged (341 configurations are required to account for 99% of the final entropy estimate). They are not well converged when the 500 frames are collected over a period of only 2.5 ns (403 configurations are required to account for 99% of the final entropy estimate). This is an indication that the conformational space of aliphatic chains is sampled more slowly within a lipid bilayer than in a pure liquid alkane at the same temperature. A similar behavior is found when comparing single-chain entropies

TABLE 2: Single-Chain Configurational Entropies from MD Simulations (AL Model) of Lipids in a DPPC Bilayer at 323 K^a

acyl chain	S_{ch}^{i} (ch)	$S_{\text{ch}}^{\text{ir}}$ (ch)	$S_{\text{ch}}^{\text{ip}}$ (ch)	$S_{\text{ch}}^{\text{irp}}$ (ch)	no. atoms in fit	s_{ch}^{r} (ch)	time period (ns)	no. configs	procedure
	(J K ⁻¹ mol ⁻¹)					(%)			
DPPC sn1	790	936	49	58	16	15	2.5	500	ave
	803	974	50	68	16	17	25	500	ave
	816	994	51	62	16	18	400	8000	con1
	821	994	51	62	16	17	400	8000	con2
DPPC sn2	791	929	49	67	16	15	2.5	500	ave
	810	980	51	68	16	17	25	500	ave
	822	1002	51	63	16	18	400	8000	con1
	823	1002	51	63	16	18	400	8000	con2

^a Entropies are calculated using different superpositional fitting procedures and different numbers of configurations collected over different simulation time periods. The number of atoms used for the fitting and the relative contribution s_{ch}^{r} of overall rotation to the absolute entropy are also reported. Two types of entropy estimates are given: (i) averages (ave) over the entropies of the 64 lipids in the first leaflet and (ii) entropies for the concatenated trajectories of 16 chains from the first (con1) or the second (con2) DPPC leaflet. Standard deviations around the average are smaller than 0.5 J K⁻¹ mol⁻¹ in all cases. See Table 1 for definition of entropy reference codes and Methods section for configurational entropy nomenclature.

of *cis*-9-octadecene (C18:c9) chains in the liquid phase and in DOPC lipid tails (not shown).

A more detailed analysis of the convergence properties of the configurational entropy is given in Table 2, which reports the single-chain internal S^{i} as well as internal plus rotational S^{ir} entropies for the sn1 and sn2 lipid tails of a DPPC bilayer at 323 K in the AL model, averaged over all 64 lipids of one leaflet (procedure ave). For both S^{i} and S^{ir} small increases in magnitude can be noticed upon increasing the time period used for the entropy calculation. On the basis of an empirical evaluation of the intrinsic accuracy of the quasi-harmonic method for systems of the type considered here,⁸⁶ we consider as insignificant changes in entropy smaller than 2% of the calculated value. S^{i} entropies are lower for sn1 and sn2 tails than for the corresponding C16 hydrocarbon chains in the liquid phase (i.e., 842 J K⁻¹ mol⁻¹; see ref 90). The values are systematically slightly larger for sn2 tails than those for sn1 tails, an indication of the comparatively higher mobility of the sn2 chain. This observation is at odds with a previous suggestion³⁵ made on the basis of experimental order parameters for dimyristoylphosphatidylcholine (DMPC) and distearoylphosphatidylcholine (DSPC). (After numerical deconvolution of the solid-state ²H NMR doublets,¹⁰¹ assignments are made to the methylene groups of the sn2 tails based on selective deuteration experiments; the remaining signal is then attributed to specific methylene groups of the sn1 tails; see ref 35.) However, this difference in the single-chain configurational entropies S^{i} of the two acyl tails is consistent with the order parameters calculated from the same MD simulations.⁴⁴ This apparent discrepancy between experimental order parameters and single-chain configurational entropies may be explained considering that (i) the systematic differences in entropy estimates are generally close to the limit of accuracy of the method employed, so that the data should not be over interpreted, (ii) the lipid systems studied are not identical (DPPC and DOPC versus DMPC and DSPC), (iii) experimental results rely on peak assignments based on singly deuterated lipid chains (after assigning an NMR peak to the sn2 tails, the remaining signal is assumed to belong to the sn1 tails; see ref 35), but not all carbon atoms of the acyl chains are equally well resolved. Point ii is likely to be of minor relevance because all lipids considered share a common headgroup (PC). The same trends are observed for both S^{i} and S^{ir} values. The values are larger for sn2 tails compared to those for sn1 tails, indicating comparatively higher rotational contributions. In the AL bilayer system, rotational motions account for about 17% of the single-chain entropies for both sn1 and sn2 tails, which is smaller than the corresponding relative contribution previously found for

liquid C16 chains (19%, Table 3 in ref 90). The lower percentage of 15% obtained from 2.5 ns simulations is probably due to the fact that rotational motions are not fully sampled during this shorter simulation time. As a consequence, the difference between results from 500 configurations over 2.5 and 25 ns is larger for S^{ir} than that for the corresponding S^{i} entropies (Table 2).

To obtain more accurate results, configurational entropies were also calculated from the concatenated trajectories of 16 randomly chosen lipids from one DPPC leaflet (procedures con1 and con2, corresponding to lipids from the first or second leaflet, respectively). Table 2 shows the obtained values from ensembles of 8000 structures equivalent to 400 ns of MD simulation. Only a small (1.5%) increase in S^{i} values is found, indicating that internal contributions to the configurational entropy are already well sampled after 25 ns of simulation for the lipid tails. A slightly larger (2%) increase is found for S^{ir} values. The ranking in configurational entropies between sn1 and sn2 tails is maintained.

Single-Fragment Configurational Entropies of Acyl Chains in Pure Lipid Bilayers (AL Model). Single-fragment configurational entropies S^{i} and S^{ir} for acyl chains in lipid bilayers can be compared with the corresponding values previously reported⁹⁰ for hydrocarbons (i.e., DPPC versus C16 and DOPC versus C18:c9). Figure 3 shows the configurational entropies S^{i} and S^{ir} for DPPC tails in pure DPPC bilayers as well as the corresponding values for liquid C16 chains, averaged over the 128 acyl (DPPC) or hydrocarbon (C16) chains simulated. The internal configurational entropy S^{i} of DPPC sn1 and sn2 tails is similar to that of pure C16 chains at the free end of the chains (fragment D). However, the corresponding averages become smaller in proximity to the lipid headgroups (fragment A). The corresponding internal plus rotational configurational entropies S^{ir} are, as expected, larger. The distributions of single-fragment S^{i} and S^{ir} values along the C16 chains are similar. Average entropy estimates for the terminal fragments of C16 chains are larger than those of its central moiety, and their values are distributed symmetrically with respect to the center of the chain. In the case of DPPC tails the picture is different, especially when including the rotational contributions into the entropy calculation. The rotational motion of the lipid tails is significantly reduced toward the headgroup region of DPPC tails compared to the terminal fragments of liquid C16. Single-fragment entropies for the sn1 and sn2 tails are similar. Only for fragment A, higher internal entropy S^{i} is found for the sn2 tails. This shows that the systematically larger single-chain configurational entropies found for sn2 versus sn1 tails in Table 2 are due to

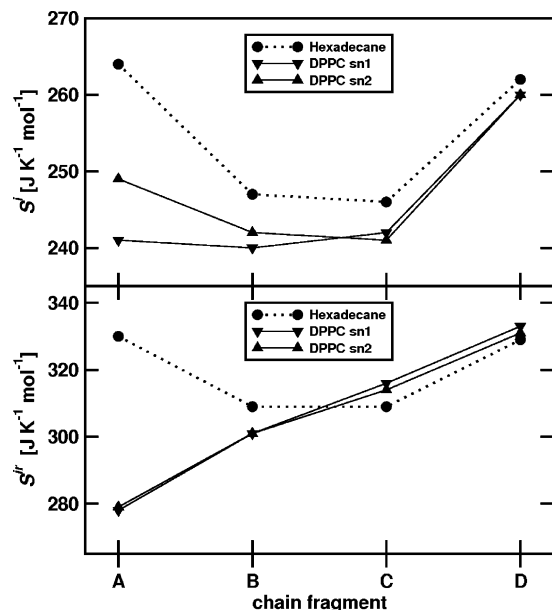


Figure 3. Comparison between single-fragment configurational entropies of DPPC lipid tails in a bilayer (L_{α} -phase) with corresponding hexadecane chains (liquid phase) at 323 K with the AL model. Internal $S_{\text{ch}}^{\text{i}}(\text{fc})$ (upper panel) and internal plus rotational $S_{\text{ch}}^{\text{i}} + S_{\text{ch}}^{\text{r}}(\text{fc})$ (lower panel) configurational entropies are shown as a function of chain fragment (Figure 1). Results for sn1 (\blacktriangledown) and sn2 (\blacktriangle) chains are given separately. Standard deviations around the average (over all molecules) are smaller than $0.5 \text{ J K}^{-1} \text{ mol}^{-1}$ in all cases. The lines are meant to guide the eye.

the specific differences in covalent connectivity in the region connecting the fragments A to the headgroup (per-fragment entropies are reported for all lipid systems investigated as Supporting Information, Table S2).

Analogous results are found for the comparison between fragments of chains in pure C18:c9 and in DOPC bilayers, although the distribution for the latter is dominated by the stiffness of the central ethylene moiety (Supporting Information, Figure S1).

Single-Chain and Single-Fragment Configurational Entropies of Acyl Chains in DOPC/DOPE Mixtures (AL Model). Table 3 reports single-chain configurational entropies of sn1 and sn2 lipid tails in mixed DOPC/DOPE and pure DOPC, DOPE, and DPPC bilayers, as calculated from MD simulations with the AL model. The configurational entropies of the sn1 and the sn2 tails in a particular system are similar for the different components of the mixture, regardless of the composition. As for pure DPPC, the internal entropy $S_{\text{sn2}}^{\text{i}}(\text{sn2})$ of the sn2 lipid tail is somewhat larger than $S_{\text{sn1}}^{\text{i}}(\text{sn1})$ for the corresponding sn1 tail. This finding agrees with the ranking of order parameters calculated from MD simulations (Figure 3 in ref 44).

Figure 4 shows the configurational entropies of sn1 and sn2 DOPC or DOPE tails as a function of DOPC/DOPE mixing. The $S_{\text{sn1}}^{\text{i}}(\text{sn1})$ and $S_{\text{sn2}}^{\text{i}}(\text{sn2})$ configurational entropies for each of the two components decrease upon increasing DOPE content. This is in agreement with a corresponding reduction in the volume and area per lipid (Table 1 in ref 44). The resulting $S_{\text{ch}}^{\text{i}}(\text{ch})$ and $S_{\text{ch}}^{\text{ir}}(\text{ch})$ entropies for lipid tails in mixed bilayers are systematically smaller than the corresponding values for C18:c9 liquid hydrocarbons (i.e., 935 and $1143 \text{ J K}^{-1} \text{ mol}^{-1}$, respectively; see ref 90).

Single-chain (Table 3) and single-fragment (Table S3, Supporting Information) configurational entropies support the general picture of homogeneous lipid mixtures, in agreement with an earlier nearest-neighbor analysis.⁴⁴ The largest differences (up to 5%) among the different mixtures are found for both S^{i} and S^{ir} entropies of the A fragments. These fragments are closest to the headgroups. Thus, differences between the solute entropies of DOPC and DOPE components appear to be linked to the specific properties of the headgroups. The influence of the A fragments is evident from similar trends observed for values of chain $S_{\text{ch}}^{\text{i}}(\text{ch})$ entropies versus fragment A $S_{\text{ch}}^{\text{i}}(\text{A})$ values as a function of mixture composition (cf. Figures 4a and 4b).

Correlation between sn1 and sn2 Tail Motions in Pure and Mixed Bilayers (AL and CG models). To estimate the correlation between the motions of the sn1 and sn2 chains of

TABLE 3: Single-Chain Configurational Entropies of Acyl Chains in Lipid Bilayers of Different Composition from MD Simulations with the AL Model^a

system ^b	$S_{\text{sn1}}^{\text{i}}(\text{sn1})$	$S_{\text{sn1}}^{\text{ip}}(\text{sn1})$	$S_{\text{sn1}}^{\text{ir}}(\text{sn1})$	$S_{\text{sn1}}^{\text{irp}}(\text{sn1})$	$S_{\text{ch}}^{\text{r}}(\text{ch})$ (%)	$S_{\text{sn1}}^{\text{i}}(\text{sn2})$	$S_{\text{sn2}}^{\text{ip}}(\text{sn2})$	$S_{\text{sn2}}^{\text{ir}}(\text{sn2})$	$S_{\text{sn2}}^{\text{irp}}(\text{sn2})$	$S_{\text{ch}}^{\text{r}}(\text{ch})$ (%)
	(J K ⁻¹ mol ⁻¹)					(J K ⁻¹ mol ⁻¹)				
pure DPPC ^c	803	50	974	61	17	810	51	980	61	17
DOPC ^d	883	49	1048	58	16	892	49	1052	58	15
3:1 (48:16) mixture										
DOPC ^d	860 ± 1	48	1022 ± 1	57	16	874	48	1024 ± 1	57	15
DOPE ^d	856 ± 1	47	1018 ± 1	56	16	870 ± 2	48	1019 ± 1	57	15
1:1 (32:32) mixture										
DOPC ^d	852 ± 1	47	1015 ± 1	56	16	873 ± 1	48	1026 ± 1	57	15
DOPE ^d	852 ± 1	47	1013 ± 1	56	16	870 ± 1	48	1025 ± 1	57	15
1:3 (16:48) mixture										
DOPC ^d	831 ± 1	46	976 ± 1	54	15	851 ± 2	47	992 ± 3	55	14
DOPE ^d	836 ± 1	46	982 ± 1	54	15	852 ± 1	47	993 ± 1	55	14
pure DOPE ^e	798	44	956	53	16	822	46	965	54	15

^a The composition of each lipid mixture is given together with the number of lipids of each component per leaflet. See Table 1 for definition of entropy reference codes and Methods section for configurational entropy nomenclature. Results are averaged over all lipid tails of a particular component. Standard deviations around the average (over all tails) are also reported unless smaller than $0.5 \text{ J K}^{-1} \text{ mol}^{-1}$. ^b Each leaflet is composed of a total of 64 lipids. The corresponding composition is reported in parentheses. ^c From a 25 ns MD simulation at 323 K, 500 trajectory configurations are used for the entropy calculations. ^d From a 40 ns MD simulation at 303 K, 800 trajectory configurations are used for the entropy calculations. ^e From a 30 ns MD simulation at 303 K, 600 trajectory configurations are used for the entropy calculations.

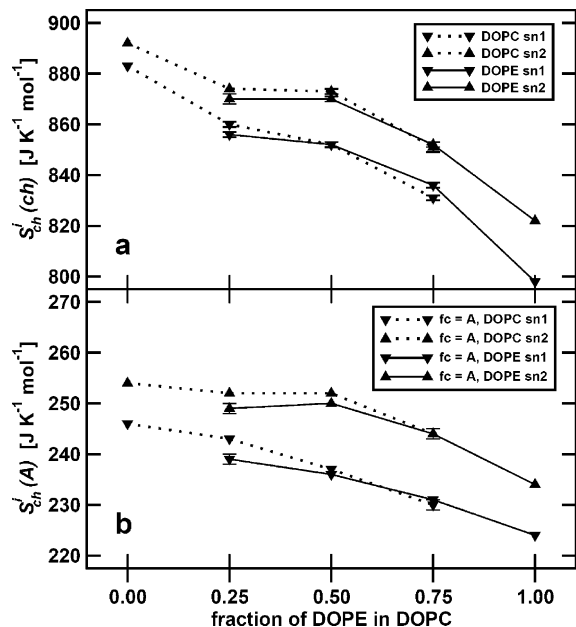


Figure 4. Configurational entropies of the sn1 and sn2 acyl chains of individual DOPC (dotted lines) and DOPE (continuous lines) in DOPC/DOPE mixtures as function of mixture composition. (a) $S_{\text{sn1}}^i(\text{sn1})$ and $S_{\text{sn2}}^i(\text{sn2})$ values account for entropies of the entire sn1 and sn2 tails, respectively (Table 3). (b) $S_{\text{sn1}}^i(\text{A})$ and $S_{\text{sn2}}^i(\text{A})$ values account for entropies of the fragments A of the sn1 and sn2 tails, respectively (Table S2 and S3, Supporting Information; see also Figure 1 for fragment definition). Results for sn1 (\blacktriangledown) and sn2 (\blacktriangle) chains are given separately. Standard deviations from the mean (over all molecules) are displayed as vertical bars. The lines are meant to guide the eye.

DPPC and DOPC lipids using eq 4, S^i and S^{ir} were also calculated using the atoms of both the sn1 and sn2 tails when

superimposing trajectory structures, yielding $S_{\text{sn1+2}}^i(\text{sn1} + 2)$ and $S_{\text{sn1+2}}^{\text{ir}}(\text{sn1} + 2)$ values (Table 4). These values, even when including the overall rotation of a lipid around its main axis ($S_{\text{sn1+2}}^{\text{ir}}(\text{sn1} + 2)$), were found to be well converged when calculated from 500 structures collected over a simulation time of 25 ns (Supporting Information, Figure S2). Table 4 gives the single-chain configurational entropies of the sn1 and sn2 tails of lipids in bilayers (averages over all lipids simulated). The overall single-chain entropies of both tails are calculated using an identical set of atoms for the superposition of configurations. The correlation entropies $S_{\text{sn1+2}}^i(\text{sn1}, \text{sn2})$ between sn1 and sn2 tails of individual lipids obtained from eq 4 are not very different among pure DPPC, DOPC, and DOPE (-202 , -208 , and $-208 \text{ J K}^{-1} \text{ mol}^{-1}$, respectively). Still, when the rotational contribution is included, a larger correlation entropy $S_{\text{sn1+2}}^{\text{ir}}(\text{sn1}, \text{sn2})$ is found for pure DOPE compared to pure DPPC and DOPC (-169 versus -59 and $-61 \text{ J K}^{-1} \text{ mol}^{-1}$, respectively). In all cases the correlation entropy is negative, which shows that the interaction between the chains reduces the extent of configurational spaces that they individually access. This reduction is considerably larger for S^i than that for S^{ir} , which implies a more significant correlation between the motions of the chains when the rotational contribution is excluded from the calculation. This can be due to the limited rotation of the lipid chains with respect to each other. We note that the correlation between sn1 and sn2 chains decreases for both components upon increasing the DOPE content.

Comparison of the AL and CG Models. The properties of DPPC and DOPC lipid bilayers were also studied at lower spatial resolution using a CG model for lipid simulations.²⁷ Figure 5 illustrates the correspondence between the AL and the CG models in terms of average structures for DPPC lipids. To

TABLE 4: Average Intramolecular Correlation between the Motions of the sn1 and sn2 Lipid Tails of Individual Lipids in Bilayers of Different Compositions from MD Simulations with the AL and CG Models^a

system ^b	$S_{\text{sn1+2}}^d(\text{sn1} + 2)$	$S_{\text{sn1+2}}^d(\text{sn1})$	$S_{\text{sn1+2}}^d(\text{sn2})$	$S_{\text{sn1+2}}^d(\text{sn1}, \text{sn2})$	$S_{\text{sn1+2}}^{\text{ir}}(\text{sn1} + 2)$	$S_{\text{sn1+2}}^{\text{ir}}(\text{sn1})$	$S_{\text{sn1+2}}^{\text{ir}}(\text{sn2})$	$S_{\text{sn1+2}}^{\text{ir}}(\text{sn1}, \text{sn2})$	time period (ns)	T (K)
	(J K ⁻¹ mol ⁻¹)				(J K ⁻¹ mol ⁻¹)					
AL model										
pure DPPC ^c	1871 ± 1	1036	1038	-202	2125 ± 1	1094	1090	-59	25	323
DOPC ^d	2040 ± 1	1122	1126	-208	2277 ± 1	1170	1168	-61	40	303
3:1 mixture										
DOPC ^d	1991 ± 1	1092 ± 1	1099 ± 1	-201	2222 ± 1	1141 ± 1	1141 ± 1	-60	40	303
DOPE ^d	1984 ± 2	1090 ± 2	1095 ± 2	-201	2205 ± 4	1136 ± 2	1133 ± 2	-54	40	303
1:1 mixture										
DOPC ^d	1985 ± 1	1083 ± 1	1095 ± 1	-193	2229 ± 1	1137 ± 1	1142 ± 1	-50	40	303
DOPE ^d	1988 ± 1	1087 ± 1	1097 ± 1	-196	2228 ± 1	1138 ± 1	1142 ± 1	-51	40	303
1:3 mixture										
DOPC ^d	1917 ± 2	1040 ± 2	1058 ± 2	-193	2138 ± 2	1097 ± 2	1097 ± 2	-55	40	303
DOPE ^d	1921 ± 1	1054 ± 1	1066 ± 2	-192	2140 ± 1	1098 ± 1	1098 ± 1	-56	40	303
pure DOPE ^e	1829 ± 1	1014	1023	-208	1979 ± 1	1070	1078	-169	30	303
CG model										
pure DPPC ^f	628	404	404	-181	899	462	455	-19	1000	323
DOPC ^g	847	524	524	-201	1012	573	577	-138	1000	303

^a Results are averaged over all lipids of a particular component. Standard deviations from the averages (over all molecules) are also reported unless smaller than $0.5 \text{ J K}^{-1} \text{ mol}^{-1}$. The composition of each lipid mixture is given together with the number of lipids of each component. See Table 1 for definition of entropy reference codes and Methods section for configurational entropy nomenclature. The correlation entropy $S_{\text{sn1+2}}^{\text{type}}(\text{sn1}, \text{sn2})$ is defined by eq 4. ^b Each system is composed of a total of 128 (AL model) or 512 (CG model) lipids. ^c From a 25 ns MD simulation of DPPC at 323 K, 500 trajectory configurations are used for the entropy calculations. ^d From a 40 ns MD simulation of DOPC at 303 K, 800 trajectory configurations are used for the entropy calculations. ^e From a 30 ns MD simulation of DOPE at 303 K, 600 trajectory configurations are used for the entropy calculations. ^f From a 1 μs MD simulation at 323 K of DPPC (CG model) of a bilayer system constituted by 128 lipids. ^g From a 1 μs MD simulation at 323 K of DOPC (CG model). Results are averages over entropies of 128 lipids out of the 512 simulated.

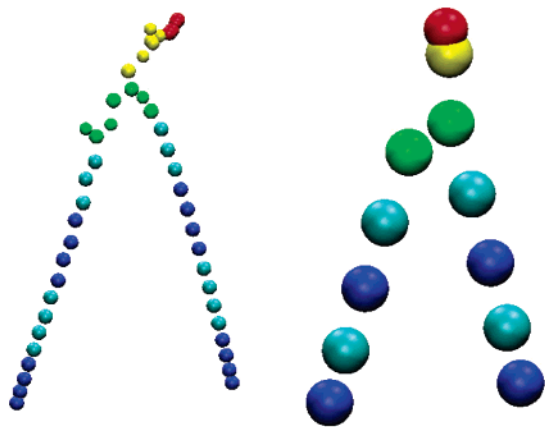


Figure 5. Average structures of a DPPC lipid from concatenated trajectories with the AL (left) and CG (right) models corresponding to a total simulation time of 25.6 and 1 μ s, respectively. The molecular models are displayed after superposition of the planes containing the average positions of the acyl atom particles. Color coding for the AL and CG models show the mapping correspondence (see also Figure 1).

enhance the sampling in the case of the AL model, the average structure was obtained from concatenated trajectories of the 64 lipids constituting one leaflet of the bilayer, from a 400 ns simulation at 323 K, which corresponds to a concatenated trajectory of 25.6 μ s (5.12×10^5 structures). In the case of the CG model a single lipid trajectory (out of the 512 in the simulated bilayer) of 1 μ s (2×10^4 structures) at 323 K was used. Although these average structures may never be sampled during the corresponding MD simulations, they contain useful information when comparing the AL and CG structural resolutions. Both the average (pseudo)-bond-angle between the acyl chains and the tilt angle of the headgroups with respect to the lipid main axis are similar in the two models.

Figure 6 reports single-chain configurational entropies $S_{\text{ch}}^{\text{i}}(\text{ch})$ and $S_{\text{ch}}^{\text{ir}}(\text{ch})$ as a function of simulation time for individual sn1 and sn2 acyl chains from 1- μ s MD simulations of 512 DPPC lipids in a bilayer at 323 K using the CG model. For graphical purposes only results from a sample selection of 32 lipids (16 randomly chosen from each bilayer leaflet) are displayed. The spread of the final estimate for the different lipid molecules considered is enhanced by the different initial configurations used in the fitting procedure to superimpose trajectory structures of the individual chains (eq 2). It amounts in the present case up to 5% ($S_{\text{ch}}^{\text{i}}(\text{ch})$) or 2% ($S_{\text{ch}}^{\text{ir}}(\text{ch})$) of the final values. This effect is similar in magnitude to that reported for other flexible molecules.⁸⁶ Both $S_{\text{ch}}^{\text{i}}(\text{ch})$ and $S_{\text{ch}}^{\text{ir}}(\text{ch})$ show good convergence behavior, and their variation over time is

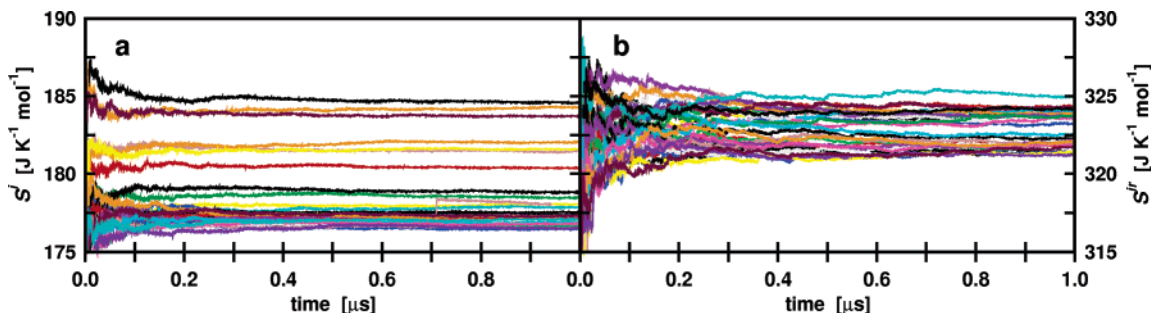


Figure 6. Single-chain configurational entropies as a function of simulation time for DPPC lipids in a bilayer (CG model). Configurational entropies (a) $S_{\text{ch}}^{\text{i}}(\text{ch})$ and (b) $S_{\text{ch}}^{\text{ir}}(\text{ch})$ are displayed (colored lines) for individual sn1 and sn2 acyl chains from a sample of 32 lipids (16 randomly chosen from each of the two leaflets) among the 512 DPPC lipids simulated at 323 K. See Table 1 for definition of entropy codes and Methods section for configurational entropy nomenclature.

TABLE 5: Single-Chain Configurational Entropies $S_{\text{ch}}^{\text{type}}(\text{ch})$ of Acyl Chains in Lipid Bilayers from MD Simulations with the CG Model^a

acyl chain ^b	$S_{\text{ch}}^{\text{i}}(\text{ch})$ $S_{\text{ch}}^{\text{ir}}(\text{ch})$ $S_{\text{ch}}^{\text{ip}}(\text{ch})$ $S_{\text{ch}}^{\text{irp}}(\text{ch})$				no. atoms in fit	$S_{\text{ch}}^{\text{r}}(\text{ch})$ (%)	T (K)
	(J K ⁻¹ mol ⁻¹)						
DPPC sn1	178	324	44	81	4	45	323
DPPC sn2	178	322	44	80	4	45	323
DOPC sn1	278	432	56	86	5	36	303
DOPC sn2	278	415	56	83	5	33	303

^a Entropies are calculated using 2500 configurations collected over 1 μ s of simulation. The number of atoms used for the superposition of chain structures (fit), the relative contribution of chain rotation to the absolute entropy $S_{\text{ch}}^{\text{r}}(\text{ch})$, and the simulation temperature are also reported. See Table 1 for definition of entropy reference codes and Methods section for configurational entropy nomenclature. ^b Results are averages over entropies for 64 lipids from one leaflet of the 128 (DPPC) or 512 (DOPC) lipids simulated. Standard deviations around the averages (over all molecules) are smaller than 0.5 J K⁻¹ mol⁻¹.

small compared to the corresponding lipid systems simulated using the AL model (compare Figure 6 and Figures 2c and 2d). This result is expected in view of the reduced number of degrees of freedom present in the CG model and the longer time period of simulation considered (1 μ s versus 25 ns). Values of $S_{\text{ch}}^{\text{ir}}(\text{ch})$ are always larger than the corresponding $S_{\text{ch}}^{\text{i}}(\text{ch})$ values, as previously observed in the case of the AL model (Table 2).

Table 5 reports the single-chain configurational entropies for the lipid tails in DPPC and DOPC lipid bilayers (CG model). Both $S_{\text{ch}}^{\text{i}}(\text{ch})$ and $S_{\text{ch}}^{\text{ir}}(\text{ch})$ entropy values are expected and found to be smaller than those of the corresponding CG hydrocarbons (i.e., C16, 179 and 341 J K K⁻¹ mol⁻¹; C18:c9, 275 and 452 J K K⁻¹ mol⁻¹, respectively; see ref 90). For the entropies per particle $S_{\text{ch}}^{\text{ip}}(\text{ch})$ similar values are found for the CG and AL models (i.e., DPPC sn1, 44 and 50 J K K⁻¹ mol⁻¹; DPPC sn2, 44 and 51 J K K⁻¹ mol⁻¹; DOPC sn1, 56 and 49 J K K⁻¹ mol⁻¹; DOPC sn2, 56 and 49 J K K⁻¹ mol⁻¹, respectively; cf. Tables 3 and 5). A lower number of degrees of freedom also modifies the influence of the rotational motions included in the $S_{\text{ch}}^{\text{irp}}(\text{ch})$ values.

A comparative analysis was also performed on a fragment/bead basis to gain insight into the matching of the results using the low-resolution CG model to those using the higher-resolution AL one. To this end we analyzed three distinct types of trajectories (i) generated using an AL model, (ii) derived from an AL simulation, mapping the center of mass of each AL fragment (see also Figure 1) to the corresponding CG bead (MAP), and (iii) generated using a CG model.

Table 6 summarizes the internal plus configurational entropies $S_{\text{ch}}^{\text{ir}}(\text{fc})$ for DPPC and DOPC lipid tails from one-component

TABLE 6: Comparison of Fragment Entropies $S_{\text{fit}}^{\text{ir}}(\text{fc})$ between theAL and CG Models for Acyl Chains^a

		sn1			sn2			model			
		AL		CG	AL		CG	AL		CG	
		$S_{\text{fc}}^{\text{ir}}(\text{fc})$	$S_{\text{sn1}}^{\text{ir}}(\text{fc})$	$S_{\text{sn1}}^{\text{ir}}(\text{fc})$	$S_{\text{fc}}^{\text{ir}}(\text{fc})$	$S_{\text{sn2}}^{\text{ir}}(\text{fc})$	$S_{\text{sn2}}^{\text{ir}}(\text{fc})$	$S_{\text{fc}}^{\text{ir}}(\text{fc})$	$S_{\text{ch}}^{\text{ir}}(\text{fc})$	$S_{\text{ch}}^{\text{ir}}(\text{fc})$	
system ^b	fc	(J K ⁻¹ mol ⁻¹)						system ^b	(J K ⁻¹ mol ⁻¹)		
DPPC ^c	A	171	117	122	183	116	117	hexadecane ^e	211	133	131
	B	191	104	126	196	103	122		209	111	110
	C	198	99	131	201	97	128		209	111	110
	D	206	122	138	209	121	136		211	133	131
DOPC ^d	A	166	115	124	173	115	123	<i>cis</i> -9-octadecene ^f	211	135	136
	B	186	103	114	187	104	114		209	117	121
	C	54	101	105	55	101	105		66	101	108
	D	197	99	110	197	101	111		209	117	121
	E	207	122	129	206	123	129		211	135	136

^a Corresponding values from their hydrocarbon template chains (ref 90) are also shown. The configurational entropy is also calculated based on the centers of mass of single fragments in the AL model (MAP), which allows for a direct comparison with the corresponding CG beads. For each fragment, the loss in entropy due to coarse-graining of the acyl and hydrocarbon chains can be estimated by comparing the AL and MAP values. For fragments (fc) nomenclature we refer to Figure 1. See Table 1 for definition of entropy codes and Methods section for configurational entropy nomenclature. Standard deviations from the average values are smaller than 0.5 J K⁻¹ mol⁻¹ (not reported). ^b Results are averaged over entropies for 128 chains. This corresponds to 2 × 64 lipids (DPPC and DOPC) or to 128 alkane molecules (hexadecane and *cis*-9-octadecene). In the case of CG *cis*-9-octadecene results are averages over 128 alkanes of the 512 simulated. ^c For AL, from a 25 ns MD simulation at 323 K, 500 trajectory configurations are used for the entropy calculations. For CG, from a 1 μs MD simulation at 323 K. ^d For AL, from a 40 ns MD simulation at 303 K, 800 trajectory configurations are used for the entropy calculations. For CG, from a 1 μs MD simulation at 303 K. Note that fragment C includes only 2 united atoms. ^e For AL, from a 25 ns MD simulation at 323 K, 500 trajectory configurations are used for the entropy calculations. For CG, from a 1 μs MD simulation at 323 K. ^f For AL, from a 25 ns MD simulation at 303 K, 500 trajectory configurations are used for the entropy calculations. For CG, from a 2.5 μs MD simulation at 303 K. Note that fragment C includes only 2 united atoms.

bilayer simulations and the corresponding C16 and C18:c9 liquid hydrocarbon chains.⁹⁰ Note that the AL entropies involve (translational) least-squares fitting of trajectory configurations based on the individual fragment, while the fitting is based on the whole chain for the CG and MAP cases. Results for the different systems are directly comparable (although they were calculated from simulations of different time lengths and using different numbers of configurations), because complete convergence was reached in both cases for the corresponding $S_{\text{ch}}^{\text{ir}}(\text{fc})$ entropies (not shown).

The comparison of AL versus MAP results provides an indication of the loss in configurational entropy upon coarse-graining the AL model.⁹⁰ The entropy loss per bead amounts to about 40–100 J K⁻¹ mol⁻¹, and it is comparable in the lipid tails and in the hydrocarbon liquids. Note that the loss in entropy depends on the fragment/bead position in the chain, partially due to the fitting procedure employed. This may be a consequence of the fact that back-folding of the chain ends occurs to a larger extent in the AL model than in the CG model, because (i) the CG beads are larger than the corresponding AL united-atom particles and (ii) back-folding requires large deviations from the equilibrium angles in the CG model but can be achieved by a number of comparatively smaller deviations of bonds, bond angles, and torsional angles in the AL model.

The MAP and CG results are directly comparable (i.e., they can be used to assess the compatibility between the AL and the CG models, in terms of configurational-space sampling and flexibility).⁹⁰ The CG model clearly provides a reasonable description of the overall hydrocarbon chain flexibility with reference to the AL model (in its mapped form) for both DPPC and DOPC lipid tails. The fragment/bead entropies of terminal regions of lipid tails or hydrocarbon chains are not too different when comparing the two models (Figure 7). Expectedly, their entropy distributions along the acyl chains differ due to different interbead (CG) and interfragment (AL) positional correlation. The central CG bead mapping the AL double bond is found to be more flexible compared to the AL model. The specific

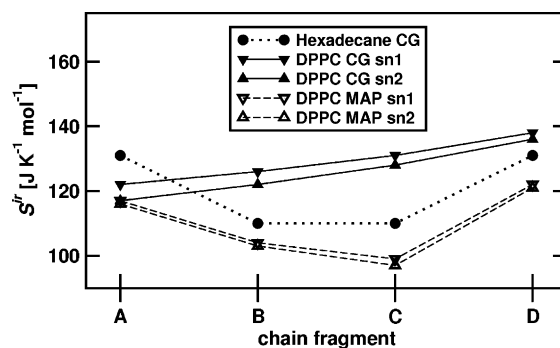


Figure 7. Comparison of fragment entropies $S_{\text{ch}}^{\text{ir}}(\text{fc})$ for DPPC lipid tails in a bilayer with corresponding values for liquid hexadecane chains in the CG model. Internal plus rotational configurational entropies are shown for consecutive fragments along the chain. Single-fragment estimates after mapping (MAP) the AL model onto the CG model are also shown. Results for sn1 (▼ and ▽) and sn2 (▲ and △) chains are given separately. Standard deviations around the average (over all molecules) are smaller than 0.5 J K⁻¹ mol⁻¹ in all cases. The lines are meant to guide the eye.

differences of sn1 and sn2 tails vanish upon coarse-graining of the model. In the case of DOPC and C18:c9 a good correspondence is found between the two models in terms of (pseudo-)bond-angle distributions around the central double bond moiety. This can be inferred, for example, from the corresponding angle distributions reported as Supporting Information, Figure S3. Larger average (pseudo-)bond-angles for the central double bond moiety characterize DOPC lipid tails compared to C18:c9 aliphatic chains in both AL and CG models.

When coarse-graining a simulation model, the number of degrees of freedom is reduced, and the potential energy function generally becomes smoother. This permits the use of larger simulation time steps (40 versus 5 fs in the present study), the production of longer trajectories, and the investigation of larger systems. However, the definition of the proper time scale for a CG model is not straightforward, as well as its correspondence to the AL model. Thus, it is of interest to investigate the mapping

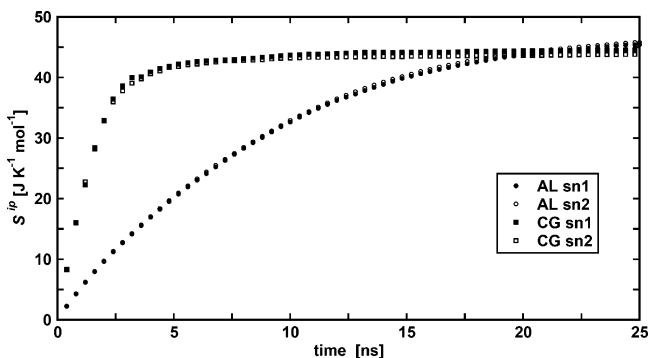


Figure 8. Single-chain internal configurational entropies per particle $S_{\text{ch}}^{\text{ip}}(\text{ch})$ for the two acyl chains sn1 and sn2 of the AL and CG models as a function of time from MD simulations of DPPC bilayers. The average (over 128 simulated molecules) values of the configurational internal entropies $S_{\text{sn1}}^{\text{ip}}(\text{sn1})$ and $S_{\text{sn2}}^{\text{ip}}(\text{sn2})$ of the lipid tails are reported.

of the CG simulation time onto the corresponding AL simulation time. This can be assessed qualitatively by a comparison between the convergence properties of the configurational entropy in the two models considered.

Figure 8 displays the build-up curves of the per-particle single-chain configurational entropies $S_{\text{ch}}^{\text{ip}}(\text{ch})$ based on the first 24.8 ns of simulations with the AL and CG models for DPPC (note that “bare” MD time scales are reported). For this analysis, entropy estimates were recalculated using the same number of 62 trajectory structures in both models to allow for a fair comparison (i.e., time intervals of 400 ps between two consecutive structures). After about 6 ns (i.e., 15 trajectory structures) the acyl DPPC sn1 and sn2 tails in the CG model already sampled their accessible configurational space. In contrast, no plateau can be observed for the AL values. Assuming full correspondence between per-particle values in the two models, a mapping of simulation times of about 4:1 can be estimated for the CG/AL comparison. The scaling of time in the CG model was estimated as about 4:1 from the self-diffusion of water and about 3:1 from the lateral diffusion of lipids.²⁷ We note that such a time-scale mapping depends on the system considered and, consequently, on the number of and the atom-positional correlation between the degrees of freedom removed when coarse-graining the simulation model. Whereas, in general, coarse-graining is expected to smoothen of the energy surface and lower barriers, the scaling may not depend linearly on the ratio of the number of particles in the AL and CG models.

Anharmonicity and Correlation Effects for DPPC Lipid Tails at AL and CG Resolutions. To evaluate anharmonicity and pairwise supralinear correlation effects, which are absent from both Schlitter and quasi-harmonic estimates of the entropy, all individual quasi-harmonic modes for the system considered

must be calculated.⁸⁶ The quasi-harmonic entropies S_{qm}^{h} , together with the associated additive corrections $\Delta S_{\text{cl}}^{\text{ah}}$ for anharmonicity in the individual modes and $\Delta S_{\text{cl}}^{\text{pc}}$ for pairwise (supralinear) correlations (both evaluated at the classical level), are reported in Table 7, from the concatenated trajectories of 64 AL or CG DPPC lipids at 323 K corresponding to total simulation times of 25.6 and 1 μs , respectively. As previously reported^{86,90} the quasi-harmonic and Schlitter estimates of the entropy are within 1% (and within 2% for all entropies reported in the present work; data not shown) from each other. A quasi-harmonic entropy⁸⁶ was also estimated for AL DPPC, restricting the calculation to its sn1 and sn2 acyl tails, and amounts to 1924 J K K⁻¹ mol⁻¹. A corresponding $S_{\text{sn1+2}}^{\text{cl}}(\text{sn1} + 2)$ value of 1926 J K K⁻¹ mol⁻¹ was obtained using the Schlitter approach (eqs 1 and 2) and the same concatenated trajectory, i.e., only 3% larger than the value of 1871 J K K⁻¹ mol⁻¹ obtained from only 25 ns of simulation (Table 4), which confirms the good convergence of the entropy calculations previously discussed.

In all cases, including both the AL and the CG models, the anharmonicity corrections $\Delta S_{\text{cl}}^{\text{ah}}$ are negative (as expected; see ref 86) and small (at most 0.09% of S_{qm}^{h}), which agrees with previous results in the context of small-sized solute molecules.^{86,102} The corresponding overall corrections $\Delta S_{\text{cl}}^{\text{pc}}$ for pairwise (supralinear) correlation effects, to be applied to anharmonicity-corrected entropy estimates $S_{\text{qm}}^{\text{h}} + \Delta S_{\text{cl}}^{\text{ah}}$, are (as expected) also negative. This correction leads to a decrease in the estimated configurational entropies (1–9% of S_{qm}^{h} depending on AL or CG model resolution and on the atoms considered; see Table 7), which also agrees with previous results in the context of two reversibly folding β -peptides in methanol⁸⁶ and disaccharides in water.¹⁰² Note, however, that this term only accounts for pairwise mode correlations. Higher-order correlations will further lower the entropy, but are increasingly difficult to estimate due to the need for more extensive sampling and increasingly expensive computations. Higher-order correlations are expected to be more relevant for highly branched molecules than for linear chains. The total correction is smaller (1% of S_{qm}^{h}) for CG DPPC lipid tails than that for corresponding AL ones ($\leq 9\%$ of S_{qm}^{h}), which is expected considering the smoother potential energy surface of the CG model.

Conclusions

In the present work, the properties of lipid tails have been studied for fully hydrated lipid bilayer systems (pure lipids and binary mixtures), on either fine-grained AL or coarse-grained CG resolution scales. The AL model provides an atomistic picture of the nature of the lipid lamellar state and permits quantification of properties (e.g., single-chain and single-fragment configurational entropies, correlation in the motion

TABLE 7: Mode Anharmonicity and Pairwise (Supralinear) Correlation Corrections to the Quasi-Harmonic Entropy Estimates for DPPC Lipids Calculated as in Ref 86 for Both Simulations with the AL and CG Models at 323 K^a

molecule	S_{qm}^{h}	$\Delta S_{\text{cl}}^{\text{ah}}$	$\Delta S_{\text{cl}}^{\text{pc}}$	S^{ctd}	no. solute atoms	time period (μs)	no. configs
	(J K ⁻¹ mol ⁻¹)						
AL DPPC ^b	2853	-1 (0.03)	-264 (9)	2588	50	25.6	256000
CG DPPC ^c	1066	-1 (0.09)	-12 (1)	1053	12	1.6	80000
AL DPPC sn1 + sn2 ^b	1924	-1 (0.05)	-72 (4)	1851	32	25.6	128000

^a The quantum-mechanical quasi-harmonic configurational entropy S_{qm}^{h} , its (classically derived) corrections for mode anharmonicities ($\Delta S_{\text{cl}}^{\text{ah}}$), and (supralinear) pairwise mode correlations ($\Delta S_{\text{cl}}^{\text{pc}}$), together with the corrected value $S^{\text{ctd}} = S_{\text{qm},o}^{\text{h}} + \Delta S_{\text{cl}}^{\text{ah}} + \Delta S_{\text{cl}}^{\text{pc}}$ are reported. For the AL model entropies are also reported for lipid tails only, to allow for a comparison with the values of Table 4. Relative values (%) of the entropy corrections (with respect to S_{qm}^{h}) are given in parentheses. See Table 1 for the entropy nomenclature. ^b Results are from 64 concatenated trajectories of all DPPC lipids composing a bilayer simulated for 400 ns. ^c Results are from 64 concatenated trajectories of DPPC lipids (out of 512 simulated) from 25 ns trajectories.

of acyl chains) otherwise not accessible to experimental measurements. The comparison between the AL and the CG models offers the possibility to investigate the effect of omitting degrees of freedom and the behavior of the underlying simplified force field. For the AL model, full sampling of the internal motions of the lipid tails in DPPC and DOPC can be reached within a simulation time of several tens of nanoseconds. For the CG model, convergence is reached for shorter simulations, at the cost of spatial resolution. If rotational contributions to the chain entropies are to be calculated, longer simulations are necessary. Still, by comparison of entropies including or excluding full rotational motions, a qualitative picture of rotational contributions arises from the approximate method employed.

Configurational entropies for fragments along the lipid tails were also calculated for DPPC and DOPC bilayer systems. A comparison with corresponding single-fragment entropy values from simulations of the hydrocarbon molecules C16 and C18: c9 in the liquid phase shows differences between the liquid phase and the L_{α} lipid phase. The acyl-chain fragment in proximity to the headgroup region is characterized by a significantly lower entropy, whereas the other chain fragments have entropy values comparable to corresponding values for hydrocarbon chains in the liquid phase. In agreement with previously calculated order parameters, sn2 chains show slightly more flexibility than sn1 chains. The same observation does not hold for comparison with NMR-derived order parameters of DMPC and DSPC. Single-chain and single-fragment configurational entropies for DOPC/DOPE are similar for the two components, suggesting homogeneous mixing behavior over the entire composition range. Changes in the configurational entropies with changes in composition are most strongly seen in the part of the lipid chain closest to the headgroup, suggesting the chemical differences in the headgroups lead to different configurational spaces available to the lipid chains.

Anharmonicity and pairwise (supralinear) correlation corrections to the quasi-harmonic entropy were estimated for a few systems at different model resolutions. While the anharmonicity correction is found to be small at both levels of description (at most 1% of the quasi-harmonic entropy), correlation effects are larger in the AL model (up to 9% of the quasi-harmonic entropy). Both effects are of comparable relative magnitude compared to those of previous studies.

The loss of configurational entropy upon coarse-graining the simulation model has been estimated by comparison between AL and CG entropies. It amounts to about 40–100 J K⁻¹ mol⁻¹ per bead for DPPC and DOPC. This effect is of comparable magnitude to that previously reported for the corresponding liquid hydrocarbons and depends on the fragment position along the chain. The CG model yields a reasonably good approximation of the distribution of entropy along the chains of the AL model (in its mapped form) for both DPPC and DOPC.

Deviations between the AL and the CG models have been observed, limited to short-range local properties. For example, the difference in entropy between the sn1 and the sn2 chains is lost upon coarse-graining, and a reduced correlation in the bead motion is found in comparison to the correlation of the united atoms, also revealed by the smaller correction for quasi-harmonic pairwise (supralinear) mode correlation effects. In general, a good correspondence is found between the AL and the CG models.

The present study showed the differences in flexibility and configurational entropy between lipid tails in fully hydrated bilayer systems and hydrocarbon liquids and demonstrated that CG models can capture the major structural and dynamical features of AL ones. This is a promising step for the use of such models in MD simulations of larger systems over longer time periods.

Acknowledgment. Financial support from the National Center of Competence in Research (NCCR), Structural Biology, of the Swiss National Science Foundation (SNSF) is gratefully acknowledged. R.B. thanks H. I. Petrache for providing insightful information on NMR spectral assignments of fluid phosphatidylcholines. The authors thank C. Anézo for making available the trajectory of the AL DPPC bilayer system described in ref 66.

Supporting Information Available: Summary of the simulated systems, single-fragment configurational entropies for DPPC, DOPC, and DOPE lipid tails in pure and multicomponent bilayers, entropy convergence plots, distributions of single-fragment configurational entropies for DOPC compared to C18: c9 for the AL and CG models, and (pseudo-)bond-angle distributions of atoms around the double bond moiety in C18: c9 chains and DOPC tails. This material is available free of charge via the Internet at <http://pubs.acs.org>.

References and Notes

- (1) Wright, P. E.; Dyson, H. J. *J. Mol. Biol.* **1999**, *293*, 321.
- (2) Dyson, H. J.; Wright, P. E. *Curr. Opin. Struct. Biol.* **2002**, *12*, 54.
- (3) Iakoucheva, L. M.; Brown, C. J.; Lawson, J. D.; Obradović, Z.; Dunker, A. K. *J. Mol. Biol.* **2002**, *323*, 573.
- (4) Dyson, H. J.; Wright, P. E. *Nat. Rev. Mol. Cell Biol.* **2005**, *6*, 197.
- (5) Davson, H.; Danielli, J. F. *Permeability of Natural Membranes*; Cambridge University Press: New York, 1952.
- (6) Singer, S.; Nicholson, G. *Science* **1972**, *175*, 720.
- (7) Israelachvili, J. N.; Marčelja, S.; Horn, R. *Q. Rev. Biophys.* **1980**, *13*, 121.
- (8) Lipowsky, R.; Sackman, R. *Structure and Dynamics of Membranes*; Elsevier: Amsterdam, NL, 1995; Vol. 1A.
- (9) Miller, A. F.; Falke, J. J. *Adv. Protein Chem.* **2004**, *68*, 394.
- (10) Yeagle, P. L. In *The Structure of Biological Membranes*, 2nd ed.; Yeagle, P. L., Ed.; CRC Press: New York, 2005; p 479.
- (11) Miller, C.; White, M. M. *Proc. Natl. Acad. Sci. U.S.A.* **1984**, *81*, 2772.
- (12) Ohki, S.; Spangler, R. A. In *The Structure of Biological Membranes*, 2nd ed.; Yeagle, P. L., Ed.; CRC Press: New York, 2005; p 329.
- (13) Ipsen, J. H.; Mouritsen, O. G.; Bloom, M. *Biophys. J.* **1990**, *57*, 405.
- (14) Wolfe, J.; Bryant, G. *Cryobiology* **1999**, *39*, 103.
- (15) Hofsäuss, C.; Lindahl, E.; Edholm, O. *Biophys. J.* **2003**, *84*, 2192.
- (16) Sum, A. K.; Faller, R.; de Pablo, J. J. *Biophys. J.* **2003**, *85*, 2830.
- (17) Villareal, M. A.; Diaz, S. B.; Disalvo, E. A.; Montich, G. G. *Langmuir* **2004**, *20*, 7844.
- (18) Skibinsky, A.; Venable, R. M.; Pastor, R. W. *Biophys. J.* **2005**, *89*, 4111.
- (19) Pereira, C. S.; Hünenberger, P. H. *J. Phys. Chem. B* **2006**, *110*, published ASAP.
- (20) Smit, B.; Hilbers, P. A. J.; Esselink, K.; Rupert, L. A. M.; van Os, N. M.; Schlijper, A. G. *Nature* **1990**, *348*, 624.
- (21) Smit, B.; Esselink, K.; Hilbers, P. A. J.; van Os, N. M.; Rupert, L. A. M.; Szleifer, I. *Langmuir* **1993**, *9*, 9.
- (22) Goetz, R.; Lipowsky, R. *J. Chem. Phys.* **1998**, *108*, 7397.
- (23) Goetz, R.; Gompper, G.; Lipowsky, R. *Phys. Rev. Lett.* **1999**, *82*, 221.
- (24) Groot, R. D.; Madden, T. J.; Tildesley, D. J. *J. Chem. Phys.* **1999**, *110*, 9739.
- (25) Shelley, J. C.; Shelley, M. Y.; Reeder, R. C.; Bandyopadhyay, S.; Klein, M. L. *J. Phys. Chem. B* **2001**, *105*, 4464.
- (26) Faller, R.; Marrink, S. J. *Langmuir* **2004**, *20*, 7686.
- (27) Marrink, S. J.; de Vries, A. H.; Mark, A. E. *J. Phys. Chem. B* **2004**, *108*, 750.
- (28) Marrink, S. J.; Risselada, J.; Mark, A. E. *Chem. Phys. Lipids* **2005**, *135*, 223.
- (29) Izvekov, S.; Voth, G. A. *J. Chem. Theory Comput.* **2006**, *2*, 637.

- (30) Seelig, A.; Seelig, J. *Biochemistry* **1974**, *13*, 4839.
- (31) Seelig, J. *Q. Rev. Biophys.* **1977**, *10*, 353.
- (32) Marqusee, J. A.; Warner, M.; Dill, K. A. *J. Chem. Phys.* **1984**, *81*, 6404.
- (33) Bloom, M. E.; Evans, E.; Mourits, O. *Q. Rev. Biophys.* **1991**, *24*, 293.
- (34) Thurmond, R. L.; Dodd, S. W.; Brown, M. F. *Biophys. J.* **1991**, *59*, 108.
- (35) Petrache, H. I.; Dodd, S. W.; Brown, M. F. *Biophys. J.* **2000**, *79*, 3172.
- (36) Marsh, D. In *Membrane Spectroscopy*; Grell, E., Ed.; Molecular Biology, Biochemistry and Biophysics 31; Springer-Verlag: Berlin, 1981; p 51.
- (37) Sackmann, E. In *Biophysics*; Hoppe, W., Lohmann, W., Markl, H., Ziegler, H., Eds.; Springer-Verlag: Berlin, 1989; Vol. 12, p 425.
- (38) Douliez, J.-P.; Léonard, A.; Dufourc, E. J. *Biophys. J.* **1995**, *68*, 1727.
- (39) Petrache, H. I.; Tu, K.; Nagle, J. F. *Biophys. J.* **1999**, *76*, 2479.
- (40) Nagle, J. F. *Annu. Rev. Phys. Chem.* **1980**, *31*, 157.
- (41) Egberts, E.; Berendsen, H. J. C. *J. Chem. Phys.* **1988**, *89*, 3718.
- (42) Tieleman, D. P.; Marrink, S. J.; Berendsen, H. J. C. *Biochim. Biophys. Acta* **1997**, *1331*, 235.
- (43) Tobias, D. J.; Tu, K.; Klein, M. L. *Curr. Opin. Colloid Interface Sci.* **1997**, *2*, 15.
- (44) de Vries, A. H.; Mark, A. E.; Marrink, S. J. *J. Phys. Chem. B* **2004**, *108*, 2454.
- (45) Nagle, J. F.; Wilkinson, D. A. *Biophys. J.* **1978**, *23*, 159.
- (46) Finkelstein, A. *Water Movement through Lipid Bilayers, Pores, and Plasma Membranes: Theory and Reality*; Wiley Interscience: New York, 1987.
- (47) Ge, M.; Freed, J. H. *Biophys. J.* **2003**, *85*, 4023.
- (48) Nagle, J. F. *Proc. Natl. Acad. Sci. U.S.A.* **1973**, *70*, 3443.
- (49) Sackmann, E.; Ruppel, D.; Gebhardt, C. In *Liquid Crystals of One- and Two-Dimensional Order*; Helfrich, W., Heppke, W., Eds.; Springer Series in Chemical Physics 11; Springer-Verlag: Berlin, 1986; p 309.
- (50) Cevc, G.; Marsh, D. *Phospholipid Bilayers: Physical Principles and Models*; Wiley: New York, 1987.
- (51) Rand, R. P.; Parsegian, V. A. *Biochim. Biophys. Acta* **1989**, *988*, 351.
- (52) Evans, E. *Langmuir* **1991**, *7*, 1900.
- (53) Safran, S. A. *Statistical Thermodynamics of Surfaces, Interfaces, and Membranes*; Addison-Wesley: Reading, MA, 1994.
- (54) Lindahl, E.; Edholm, O. *Biophys. J.* **2000**, *79*, 426.
- (55) Salmon, A.; Dodd, S. W.; Williams, G. D.; Beach, J. M.; Brown, M. F. *J. Am. Chem. Soc.* **1987**, *109*, 2600.
- (56) Cooper, A. *Curr. Opin. Chem. Biol.* **1999**, *3*, 557.
- (57) Li, Z.; Raychaudhuri, S.; Wand, A. J. *Protein Sci.* **1996**, *5*, 2647.
- (58) Yang, D.; Kay, L. E. *J. Mol. Biol.* **1996**, *263*, 369.
- (59) Yang, D.; Mok, Y.; Forman-Kay, J.; Farrow, N. A.; Kay, L. E. *J. Mol. Biol.* **1997**, *272*, 790.
- (60) Wrabl, J. O.; Shortle, D.; Woolf, T. B. *Proteins: Struct., Funct., Genet.* **2000**, *38*, 123.
- (61) Wang, D. C.; Taraschi, T. F.; Rubin, E.; Janes, N. *Biochim. Biophys. Acta* **1993**, *1145*, 141.
- (62) Berger, O.; Edholm, O.; Jähnig, F. *Biophys. J.* **1997**, *72*, 2002.
- (63) Lindahl, E.; Edholm, O. *J. Chem. Phys.* **2000**, *113*, 3882.
- (64) Pastor, R. W.; Venable, R. M.; Feller, S. E. *Acc. Chem. Res.* **2002**, *35*, 438.
- (65) Chiu, S. W.; Vasudevan, S.; Jakobsson, E.; Mashl, R. J.; Scott, H. L. *Biophys. J.* **2003**, *85*, 3624.
- (66) Anézo, C.; de Vries, A. H.; Hóltje, H.-D.; Tieleman, D. P.; Marrink, S. J. *J. Phys. Chem. B* **2003**, *107*, 9424.
- (67) de Vries, A. H.; Mark, A. E.; Marrink, S. J. *J. Am. Chem. Soc.* **2004**, *126*, 4488.
- (68) de Vries, A. H.; Yefimov, S.; Mark, A. E.; Marrink, S. J. *Proc. Natl. Acad. Sci. U.S.A.* **2005**, *102*, 5392.
- (69) Saccani, J.; Castano, S.; Beaurain, F.; Laguerre, M.; Desbat, B. *Langmuir* **2005**, *20*, 9190.
- (70) Pandit, S. A.; Bostick, D.; Berkowitz, M. L. *Biophys. J.* **2003**, *85*, 3120.
- (71) Balai-Mood, K.; Harroun, T. A.; Bradshaw, J. P. *Eur. Phys. J. E* **2003**, *12*, S135.
- (72) de Vries, A. H.; Chandrasekhar, I.; van Gunsteren, W. F.; Hünenberger, P. H. *J. Phys. Chem. B* **2005**, *109*, 11643.
- (73) Shelley, J. C.; Shelley, M. Y. *Curr. Opin. Colloid. Interface Sci.* **2000**, *5*, 101.
- (74) Müller, M.; Katsov, K.; Schick, M. *J. Polym. Sci., Part B: Polym. Phys.* **2003**, *41*, 1441.
- (75) Baschnagel, J.; Binder, K.; Doruker, P.; Gusev, A. A.; Hahn, O.; Kremer, K.; Mattice, W. L.; Müller-Plathe, F.; Murat, M.; Paul, W.; Santos, S.; Suter, U. W.; Tries, V. *Adv. Polym. Sci.* **2000**, *152*, 41.
- (76) Müller-Plathe, F. *ChemPhysChem* **2002**, *3*, 754.
- (77) Kremer, K. *Macromol. Chem. Phys.* **2003**, *204*, 257.
- (78) Tozzini, V. *Curr. Opin. Struct. Biol.* **2005**, *15*, 144.
- (79) Yamamoto, S.; Hyodo, S. *J. Chem. Phys.* **2003**, *118*, 7937.
- (80) Shelley, J. C.; Shelley, M. Y.; Reeder, R. C. *J. Phys. Chem. B* **2001**, *105*, 9785.
- (81) Marrink, S. J.; Mark, A. E. *J. Am. Chem. Soc.* **2003**, *125*, 11144.
- (82) Marrink, S. J.; Mark, A. E. *J. Am. Chem. Soc.* **2003**, *125*, 15233.
- (83) Karplus, M.; Kushick, J. *Macromolecules* **1981**, *17*, 325.
- (84) Di Nola, A.; Berendsen, H. J. C.; Edholm, O. *Macromolecules* **1984**, *17*, 2044.
- (85) Edholm, O.; Berendsen, H. J. C. *Mol. Phys.* **1984**, *51*, 1011.
- (86) Baron, R.; van Gunsteren, W. F.; Hünenberger, P. H. *Trends Phys. Chem.*, in press.
- (87) Schlitter, J. *Chem. Phys. Lett.* **1993**, *215*, 617.
- (88) Andricioaei, I.; Karplus, M. *J. Chem. Phys.* **2001**, *115*, 6289.
- (89) van Gunsteren, W. F.; Billeter, S. R.; Eising, A. A.; Hünenberger, P. H.; Krüger, P.; Mark, A. E.; Scott, W. R. P.; Tironi, I. G. *Biomolecular Simulation: The GROMOS96 Manual and User Guide*; vdf Hochschulverlag AG an der ETH Zürich, BIOMOS b.v.: Zürich, Switzerland, Groningen, The Netherlands, 1996.
- (90) Baron, R.; de Vries, A. H.; Hünenberger, P. H.; van Gunsteren, W. F. *J. Phys. Chem. B* **2006**, *110*, 8464.
- (91) van der Spoel, D.; van Buuren, A. R.; Apol, M. E. F.; Meulenhoff, P. J.; Tieleman, D. P.; Sijbers, A. L. T. M.; Hess, B.; Feenstra, K. A.; Lindahl, E.; van Drunen, R.; Berendsen, H. J. C. *GROMACS User Manual*, version 3.1.1; Groningen, The Netherlands, 2002. <http://www.gromacs.org/>
- (92) Berendsen, H. J. C.; Postma, J. P. M.; van Gunsteren, W. F.; Hermans, J. In *Intermolecular Forces*; Pullman, B., Ed.; Reidel: Dordrecht, The Netherlands, 1981; p 331.
- (93) Berendsen, H. J. C.; Postma, J. P. M.; van Gunsteren, W. F.; Di Nola, A.; Haak, J. R. *J. Chem. Phys.* **1984**, *81*, 3684.
- (94) Hockney, R. W. *Methods Comput. Phys.* **1970**, *9*, 136.
- (95) Hess, B.; Bekker, H.; Berendsen, H. J. C.; Fraaije, J. G. E. M. *J. Comput. Chem.* **1997**, *18*, 1463.
- (96) van Gunsteren, W. F.; Berendsen, H. J. C. *Angew. Chem., Int. Ed.* **1990**, *29*, 992.
- (97) Tironi, I. G.; Sperb, R.; Smith, P. E.; van Gunsteren, W. F. *J. Chem. Phys.* **1995**, *102*, 5451.
- (98) McLachlan, A. D. *J. Mol. Biol.* **1979**, *128*, 49.
- (99) Schäfer, H.; Mark, A. E.; van Gunsteren, W. F. *J. Chem. Phys.* **2000**, *113*, 7809.
- (100) Schäfer, H.; Daura, X.; Mark, A. E.; van Gunsteren, W. F. *Proteins: Struct., Funct., Genet.* **2001**, *43*, 45.
- (101) Bloom, M.; Davis, J. H.; Mackay, A. L. *Chem. Phys. Lett.* **1981**, *80*, 198.
- (102) Pereira, C. S.; Kony, D.; Baron, R.; Müller, M.; van Gunsteren, W. F.; Hünenberger, P. H. *Biophys. J.* **2006**, *90*, 4337.